Effects of model size and free stream nuclei on tip vortex cavitation inception scaling

Young Shen*, Georges Chahine**, Chao-Tsung Hsiao**, and Stuart Jessup*
*NSWCCD, West Bethesda, MD, USA
** Dynaflow, Inc., Jessup, MD, USA. info@dynaflow-inc.com

Abstract

Because of the complexity of the flow field in a trailing vortex, prediction of tip vortex cavitation inception on a hydrofoil or a propeller still relies heavily on model tests and application of cavitation scaling. Experiments indicate that the major parameters influencing tip vortex cavitation inception are fluid viscosity (Reynolds number) and free stream nuclei (Weber number). A scaling method based on these two parameters has been developed in this paper. Size effects on circulation, vortex cores thickness and pressure distributions in a full-scale trailing vortex are predicted from model data based on a Reynolds scale similarity flow solution. Nuclei effect on tip vortex cavitation inception is obtained from cavitation scaling and expressed in a term called G. For prescribed pressure fields in the trailing vortex, a modified Rayleigh-Plesset bubble equation is used to evaluate effects of free stream bubbles on cavitation inception. Bubble radius history and acoustic pressure are computed for various initial bubble sizes and different release locations into the vortex core. A method based on the acoustic pressure sigma gradient is introduced to define cavitation inception. The values of G at cavitation inception are obtained. Depending on the ratio of initial bubble sizes between model and full-scale waters, the nuclei effect on tip vortex cavitation inception can be greater, equal or less than one.

1 Introduction

A system of trailing vortex is associated with a finite lifting surface. When the pressure on the axis of a trailing vortex reaches a value equal to or below the vapor pressure of the flowing liquid, cavitation occurs. On a typical marine propeller, cavitation initiates first in the trailing vortex then on the blade surface. Because of the radiated noise associated with cavitation, ability to predict the onset of tip vortex cavitation is a major interest in the marine industry. Because of the complexity of the flow field in a trailing vortex, prediction of tip vortex cavitation inception on a hydrofoil or a marine propeller still relies heavily on model tests and application of cavitation scaling.

McCormick [1954, 1962] conducted a series of model tests on tip vortex cavitation inception with different planforms, model sizes, aspect ratios and airfoil section profiles. He found experimentally that the cavitation inception index σ_i increased with a power of the Reynolds number, $Re^{0.35}$. A more recent experimental study by Fruman et al [1991] gave σ_i to increase with Reynolds number $Re^{0.40}$. Currently different values of the Reynolds number power are in use at various laboratories. Further discussions of viscous effect on tip vortex are referred to Green [1988] and Arndt [1981].

Experimental data also show that tip vortex cavitation inception is sensitive to the available nuclei in the test condition [Liu and Brennen 1998]. Let σ_{if} and σ_{im} denote the tip vortex cavitation inception number on full-scale and model, respectively. The 19th ITTC cavitation committee [1990] suggested an inception scaling of $\sigma_{if} / \sigma_{im} = K (Re_f/Re_m)^n$, where n and K are empirical factors. The factor K was introduced to represent the nuclei effect. However, the values of n and K were not specifically recommended in this report. Experimental data show that the inception index approaches a limiting value as the air content is systematically increased. Often the value of K is set to 1 in many laboratories. It is assumed that if the model is tested at high air content, nuclei effect on cavitation inception disappears. Unfortunately, this assumption is not justifiable. Theoretical calculations [Ceccio and Brennen 1992] show that it is the bubble size distribution and bubble size concentration, not the dissolved air content, which is responsible for cavitation inception. Furthermore, it is shown in this paper that the nuclei effect on cavitation inception scaling is related to the respective bubble size distribution and bubble size concentration responsible for cavitation in a laboratory and ocean environment.

The difficulties in using the existing scaling method mentioned above are:

(1) what is the value of n to be used from a laboratory test to full-scale?
(2) what is the value of K to be used to quantify the nuclei effect in cavitation inception scaling?

In this paper, we present a simplified method to derive a tip vortex cavitation inception scaling formula, which addresses the above two issues.

2 Problem Formulation and Approach of Solution

Model experiments: Consider a test case with an elliptical hydrofoil model of the NACA 0020 section profile. Let b_m and c_{mmax} denote the foil span and the maximum chord length at the mid-span. The vortex roll-up process in a tip vortex core is complex [Fruman 1991, 1994]. For simplicity, Fig 1 shows a sketch of an elliptical hydrofoil with simplified trailing vortex. The model is set at an angle of attack α_m. Let V_{om} denotes the reference velocity in the test section. The pressure in the test section is then lowered slowly. When the pressure in the test section is lowered to a certain pressure, cavitation inception is detected acoustically or visually in the trailing vortex. This corresponding pressure is termed reference pressure P_{om}. The cavitation number based on these reference velocity, reference pressure and angle of attack is termed cavitation inception index σ_{im}. It is understood that the definition of cavitation inception differs among the researchers and the test engineers. A method based on the slope versus σ_{im} of the acoustic pressure to be discussed later will be used in this paper to define cavitation inception.

Full-scale cavitation: Let λ denote a linear ratio or scale ratio of the full scale to the model; namely $b_f = \lambda\, b_m$ and $c_{f\ max} = \lambda\, c_{mmax.}$ To simplify the discussion, consider a case where the full-scale trial is carried out at a ship speed V_{of} equal to the model speed V_{om}, and angle of attack α_f equals to α_m; namely $V_{of} = V_{om}$ and $\alpha_f = \alpha_m$. The question to be addressed in this paper is what is the ambient pressure P_{of} (or depth) at which tip vortex cavitation is to be detected at full-scale? The purpose of this study is to derive a simple formula to relate σ_{if} to σ_{im}.

The vortex core is a low pressure zone. A bubble entering a vortex core will experience growth and collapse in response to the pressure distribution in the vortex core. Acoustic pressure is radiated. The pressure field in the vortex core plays a major role in cavitation inception when nuclei are available. Information of the pressure distributions in the vortex cores for both model and full-scale are needed. It is assumed that the pressure distributions in the vortex core of the model are given, the pressure distributions in the full-scale vortex core will be derived on a similarity flow solution.

Since both model and full-scale have the same planform and section profiles, geometric similarity is preserved. For simplicity, assume that the incoming flows for both the model and full-scale are uniform and that the angle of attack on both foils is the same. The kinematic similarity is satisfied. It is known that the pressure distributions and the vortex core dimension are sensitive to Reynolds scaling. The dynamic similarity flow solution based on Reynolds scale will be used to derive pressure distributions between full-scale and model. It is further assumed that the presence of the bubbles in the flow does not alter the pressure distributions from the flow solution.

Growth and collapse of a given initial bubble in vortex core are computed by using DYNAFLOW's bubble dynamic code [Hsiao et al, 2000, Hsiao et al, 2001]. In this paper, the bubble is assumed to remain spherical. The bubble radius history and the corresponding acoustic pressure are computed. Cavitation inception is determined numerically by a criterion based on the slope of acoustic pressure. The nuclei effect on vortex cavitation between full-scale and model is quantified by the numerical calculations.

3 Circulation Distributions in a Trailing Vortex

Model: Extensive measurements of tip vortex roll-up and tip vortex cavitation on an elliptical planform hydrofoil have been carried out by Fruman et al [1991, 1994, 1998]. Velocities in the vortex core were measured by a two component Laser Doppler Velocimeter (LDV). Their measured tangential velocity distributions show good agreement with the Burgers [1948] two-parameter profile. It is noted that Burgers model to be used in this paper is a slight modification of the Rankine vortex model. Let $a_{cm}\,(x/c_{mmax})$ and $\Gamma_m\,(x/c_{mmax})$ denote a mean radius and circulation of the vortex core, respectively. x denotes the axial distance from the foil tip along the vortex core. Assumed circulation, core size, and pressure distributions in the trailing vortex of a model as a function of x are given in Fig 2. It is noted that the model data shown in Fig 2 are used as an example to show the procedure in deriving the tip vortex cavitation inception scaling.

Full-scale: Let s denote a non-dimensional spanwise coordinate variable given by $s \equiv y/b$ (see Fig 1). The foil span is normalized to be 1. Let c(s) denotes the chord size distribution on the foil surface along the span. Let L(s) denotes the section lift force along the foil span. The non-dimensional section lift coefficient $C_L(s)$ is given by

$$C_L(s) = L(s)/[(0.5\,\rho\,V_o^2)\,c(s)], \tag{1}$$

where ρ is the fluid density and Vo is the reference velocity. Consider high Reynolds number cases with the boundary layer on foil surfaces to be turbulent for both model and full-scale. With geometric and kinematics similarities satisfied, it is reasonable to assume that section lift coefficient distributions between the model and full-scale are identical; namely

$$C_{Lf}(s) = C_{Lm}(s). \tag{2}$$

Let $\gamma(s)$ denotes the bound vortex distributions along the span of the foil. The section lift is related to the bound vortex by

$$L(s) = \rho V_o\, \gamma(s). \tag{3}$$

Note that in some foils, the lift coefficients between the model and full-scale may exhibit slight dependency on Reynolds scale [Abbott and Von Doenhoff, 1959]. This viscous effect on lift can be incorporated in the cavitation scaling formula by modifying the bound vortex given in Equation 2.

From equations (1) to (3), we obtain the bound vortex by

$$\gamma_f(s)/V_{of} = \gamma_m(s)/V_{om}\, c_f(s)/c_m(s) = \lambda\, \gamma_m(s)/V_{om} . \quad (4)$$

This equation relates the bound vortex between the model and full-scale. The rate of change of bound vortex along the span gives the trailing vortex. Since geometric and kinematics similarities are satisfied, it is reasonable to assume that the dynamic process of tip vortex roll-up is preserved between the model and full-scale.

Full-scale: The circulation distributions along the trailing vortex Γ in the downstream direction can be expressed by

$$\Gamma_f(x/c_{fmax})/V_{of} = \lambda\, \Gamma_m(x/c_{mmax})/V_{om} . \quad (5)$$

As an example, consider a case with a linear scale ratio of $\lambda = 4$. The full-scale circulation distribution in the vortex core derived from Equation 5 is plotted in Fig 2.

4 Core Size Distribution in a Trailing Vortex

Model: It is understood that the vortex core is not symmetric. We can use Liang and Ramprian's approach [1991] or Fruman's approach [1991] to define an averaged vortex core radius. Let a_{cm} (x/c_{mmax}) denote the radius of a trailing vortex. Visual observation by Liang and Ramprian and flow velocity measurements by Fruman shows strong dependency of vortex core size on Reynolds numbers. The core size becomes smaller as the Reynolds number is increased. This is in agreement with McCormick's classic work.

McCormick [1991] showed that tip vortex cavitation inception indices differed noticeably when roughness was applied on the pressure side of the foil surface. He suggested that the vortex core thickness is related to the thickness of the boundary layer on the pressure side of the foil. This assumption is well supported by Fruman's LDV measurements. Furthermore, Fruman's measurements showed that the boundary layer growth on the pressure side of the foil surface exhibited the same characteristics of a flat plate in terms of Reynolds scale dependency.

Let δ_m denote the boundary layer thickness at the foil trailing edge. For a velocity profile expressed in $1/7^{th}$ power law, the turbulent boundary layer thickness on a flat plate is given by $\delta = 0.37 x Re^{-0.2}$ [Abbott and Von Doenhoff, 1959]. As discussed above, the boundary layer growth in the pressure side of an airfoil exhibits the same dependency on Reynolds scale as a flat plate. We obtain

$$a_{cm}/c_{mmax} \sim \delta_m/c_{mmax} \sim Re_m^{-0.2} . \quad (6)$$

At high Reynolds number with turbulent boundary layer on the foil surface, the vortex core thickness decreases with increase in Reynolds number by $Re^{-0.2}$.

Full-scale: Let δ_f denote the boundary layer thickness at the foil trailing edge.

$$a_{cf} / c_{fmax} \sim \delta_f / c_{fmax} \sim Re_f^{-0.2} . \quad (7)$$

From the similarity flow assumption, the proportionality constants given in Equations 6 and 7 are the same. We have

$$a_{cf} / a_{cm} = \lambda\, (Re_f / Re_m)^{-0.2} . \quad (8)$$

A rotating disk: Let ω and r denote the angular velocity and a radial distance from the axis. The flow in a rotating disk becomes turbulent at large Reynolds numbers, $Re = r(r\omega)/\nu$, in the same way as the flow about a plate [Schlichting 1979]. With the balance of viscous and centrifugal forces, the boundary layer thickness is given by $\delta = 0.526\, r\, Re^{-0.2}$. It is noted that the boundary layer on a rotating disk exhibits the same dependency on Reynolds scale as a plate of $Re^{-0.2}$. This observation seems to indicate that the similarity flow solutions on vortex core size based on a stationary foil may be applicable to a rotating foil.

5 Pressure Distributions in a Trailing Vortex

Model: Let C_p denote the mean pressure coefficient in a vortex core normalized by the free stream velocity V_o. In studying the cavitation inception scaling, the pressure distributions in the model vortex core C_{pm} is assumed to be given. As an example, by assuming that the radial momentum is preponderant, the pressure coefficient $C_{pm}(x/cmax)$ on the axis of the vortex can be computed by

$$C_{pm}(x/c_{mmax}) = -\int (V_{tm}(x/c_{mmax})^2/r)\, dr, \quad (9)$$

where V_{tm} and r denote the tangential velocity and radial coordinate in the vortex core. The computed pressure coefficient distribution is shown in Fig 2.

Full-scale: Note that $V_{tmax} \sim \Gamma / 2\pi a_c$. The equation 9 gives

$$C_p \sim (\Gamma / a_c V_o)^2 . \quad (10)$$

From equations 8 and 10, we have

$$C_{pf} / C_{pm} = (\Gamma_f/\Gamma_m)^2 (a_{cm}/a_{cf})^2 (V_{om}/V_{of})^2 = (Re_f / Re_m)^{0.4} . \quad (11)$$

Experimental measurements by Fruman showed that measured tip vortex cavitation inception σ_i increased with Reynolds number $Re^{0.40}$. Since σ_i is related to the minimum pressure - C_{pmin} , the equation 11 is in good agreement with Fruman's cavitation inception measurements. Full-scale pressure distributions are also plotted in Fig 2.

6 Cavitation Inception Scaling

Ideal flow case: Let C_{pmin} denotes the minimum pressure coefficient. In the ideal case, it is assumed that bubbles responsible for cavitation inception are abundant both in model and full-scale environment; namely bubble effect on cavitation is not considered in this ideal case. Furthermore, it is assumed that the pressure fields obtained form one phase flow is not altered by the presence of micro-bubble. Cavitation inception is assumed to occur when the minimum pressure coefficient reaches the vapor pressure. We have

$$\sigma_{if}*/\sigma_{im}*=- C_{pminf} /- C_{pminm} = (Re_f / Re_m)^{0.4} \quad . \tag{12}$$

As discussed above, this scaling formula agrees with Fruman's measurements [1991]. If boundary layers on model and full-scale are both turbulent, tip vortex cavitation inception is related to the minimum pressure coefficient, which in turn is related to $Re^{0.4}$[Fruman 1991].

Real flow case: It is well known that cavitation inception σ_i does not occur at - C_{pmin} instead it is generally found to occur later at -(C_{pmin} +$\Delta\sigma$), namely,

$$\begin{aligned}\sigma_{if}/\sigma_{im} &= (- C_{pminf} - \Delta\sigma_f) /(- C_{pminm} - \Delta\sigma_m) \\ &= (- C_{pminf} /- C_{pminm}) [1+ \Delta\sigma_f /- C_{pminf}]/ [1+ \Delta\sigma_m /- C_{pminm}] \\ &\equiv (- C_{pminf} /- C_{pminm}) G = G (Re_f / Re_m)^{0.4},\end{aligned} \tag{13}$$

where

$$G \equiv[1+ \Delta\sigma_f /- C_{pminf}]/ [1+ \Delta\sigma_m /- C_{pminm}] . \tag{14}$$

The term G represents the effect of gas bubbles on cavitation inception between the full-scale and model. As noted in Eq 14, the value of G can be greater, equal to or less than 1, depending on the relative effect of tensile strength of available gas bubbles between the model and full-scale. DYNAFLOW's bubble dynamic code (Hsiao, Chahine and Liu, 2001) will now be used to evaluate the values of G.

7 G Values

Pressure field: To evaluate the value of G, the pressure distributions and gas bubbles responsible for cavitation inception must be known a priori for both model and full-scale. Since the purpose of this study is to derive a cavitation scaling formula. The pressure field in the model tip vortex is given and shown in Fig 2. The scaled pressure field for the full-scale for a geometric scale ratio of λ =4 is also shown in Fig 2. The axial velocities for both model and full-scale are assumed to be the same as well as the reference velocities which are Vof = Vom = 13 m/s. Since extensive calculations are performed on this set of pressure distributions, some of the G values obtained from this set of data are discussed in this paper.

Burger Vortex Model: As described earlier, the tip vortex is approximated using the Burger's vortex model in which the tangential velocity and pressure are defined as:

$$V_t(r) = \frac{\Gamma}{2\pi r}\left(1 - e^{x_1}\right), \tag{15}$$

$$p_\omega(r) = p_\infty + \frac{1.255\rho\Gamma^2}{8\pi^2 {a_c}^2}\left\{\frac{1}{x_1}\left(1 - e^{-x_1}\right) + 2\left[E_1(x_1) - E_2(2x_1)\right]\right\}. \tag{16}$$

$$x_1 = 1.255\left(\frac{r}{a_c}\right)^2 \tag{17}$$

where p_∞ is the ambient pressure, r is the distance to the vortex center, a_c is the vortex core radius, E_1 and E_2 are exponential integrals. Equations 15 and 16 provide the tangential velocity and pressure field according to streamwise distribution of the circulation Γ and vortex core radius a_c . To complete the model for the velocity filed, the axial velocity is assumed to be constant.

8 Improved Spherical Bubble Dynamics Model

The behavior of a spherical bubble in a pressure field is usually described with a relatively simple bubble dynamics model known as the Rayleigh-Plesset equation (Plesset 1948)

$$R\ddot{R} + \frac{3}{2}\dot{R}^2 = \frac{1}{\rho}\left(p_v + p_g - p - \frac{2S}{R} - \frac{4\mu}{R}\dot{R} \right), \tag{18}$$

where R is the time dependent bubble radius, ρ is the liquid density, p_v is the vapor pressure, p_g is the gas pressure inside the bubble, p is the ambient pressure local to the bubble, μ is the liquid viscosity, S is the surface tension. If the gas is assumed to be perfect and to follow a polytropic compression relation, then one has the following relationship between the gas pressure and the bubble radius:

$$p_g = p_{g0}\left(\frac{R_0}{R} \right)^{3k}, \tag{19}$$

where p_{g0} and R_0 are the initial gas pressure and bubble radius respectively and k is the polytropic gas constant. In Equation 18 the bubble grows principally in response to a change in the ambient pressure through gaseous expansion and increase in the vaporous mass within the bubble (the vapor pressure is assumed to remain constant). In this modeling the effect of the underlying flow is only to produce a prescribed pressure field through which the bubble is passively convected, i.e. the influence of the bubble on the liquid flow is neglected.

In addition, Equation 18 does not take into account the effect of any slip velocity between the bubble and the carrying liquid. To account for this slip velocity, an additional pressure term, $\rho(\vec{U} - \vec{U}_b)^2 / 4$, is added to the classical Rayleigh-Plesset equation as:

$$R\ddot{R} + \frac{3}{2}\dot{R}^2 = \frac{1}{\rho}\left[p_v + p_{g0}\left(\frac{R_0}{R} \right)^{3k} - p - \frac{2S}{R} - \frac{4\mu}{R}\dot{R} \right] + \frac{\left(\vec{U} - \vec{U}_b\right)^2}{4}. \tag{20}$$

The above equations 18 and 19 are valid when the liquid is incompressible. However, liquid compressibility becomes important when bubble-wall velocities become comparable with the speed of sound in the liquid. Compressibility effects are also important if one is interested in many cycles of the bubble dynamics in which case energy loss by acoustic emission occurs. Gilmore (1952) obtained an efficient modification of the Rayleigh-Plesset equation that takes into account liquid compressibility. We adapt Gilmore's equation and write the modified Rayleigh-Plesset equation as:

$$\left(1 - \frac{\dot{R}}{c}\right)R\ddot{R} + \frac{3}{2}\left(1 - \frac{\dot{R}}{3c}\right)\dot{R} = \frac{1}{\rho}\left(1 + \frac{\dot{R}}{c} + \frac{R}{c}\frac{d}{dt}\right)\left[p_v + p_{g0}\left(\frac{R_0}{R} \right)^{k} - p - \frac{2S}{R} - 4\mu\frac{\dot{R}}{R} \right] + \frac{\left(\vec{U} - \vec{U}_b\right)^2}{4} \tag{21}$$

where c is the sound speed.

It is known that the ambient pressure, p, applied in the classical spherical bubble model is the pressure at the bubble center in its absence, without considering pressure variation along the bubble surface. This simplification, valid for general flows, leads to unbounded bubble growth when the pressure in the vortex center is less than the vapor pressure. Previous studies usually used this as a criterion to determine the cavitation inception number. However, this criterion is based on an over-simplification that may lead to wrong predictions. Therefore, in the improved model we use here, p is taken to be the average of the outside field pressure over the bubble surface. This enables for a much more realistic description of the bubble behavior, e.g. the bubble does not continuously grow as it is captured by the line vortex. Instead, once the bubble reaches the vortex line axis, it is subjected to an increase in the average pressure as the bubble grows and this leads to a more realistic balance of the forces applied to the bubble.

9 Bubble Motion Equation

Several prominent scientist such as Basset (1888), Boussinesq (1903), Oseen (1927) has derived the motion equation of a spherical particle subjected to the force of gravity in a fluid at rest. The equation was extended by Tchen (1947) to the case of a fluid moving with variable velocity and more recently modified by Maxey and Riley (1983). By considering the forces acting on a spherical bubble with radius R the motion equation can be written as follows:

$$\rho_b V_b \frac{d\vec{U}_b}{dt} = V_b(\rho_b - \rho)\vec{g} + V_b \nabla p + \frac{1}{2}\rho A_b C_D \left(\vec{U} - \vec{U}_b\right) \mid \vec{U} - \vec{U}_b \mid + \frac{1}{2}\rho V_b \left(\frac{d\vec{U}}{dt} - \frac{d\vec{U}_b}{dt}\right) + 6A_b\sqrt{\frac{\rho\mu}{\pi}} \int_0^t \left(\frac{d\vec{U}}{d\tau} - \frac{d\vec{U}_b}{d\tau}\right) \Big/ \sqrt{t-\tau}\, d\tau \quad , \tag{22}$$

where terms with the subscript *b* are related to the bubble and those without a subscript are related to carrying fluid. V_b and A_b are the bubble volume and projected area, which are equal to $4/3\pi R^3$ and πR^2 respectively. The bubble drag coefficient C_D in Equation 22 can be determined by using the empirical equation of Haberman and Morton (1953):

$$C_D = \frac{24}{\mathrm{R_e}_b}\left(1 + 0.197\,\mathrm{R_e}_b^{0.63} + 2.6\times10^{-4}\,\mathrm{R_e}_b^{1.38}\right), \tag{23}$$

where the bubble Reynolds number is defined as

$$\mathrm{R_e}_b = \frac{2R\left|\vec{U} - \vec{U}_b\right|}{\nu}. \tag{24}$$

The physical meaning of each term in the right hand side of Equation 22 is as follows. The first term is a buoyancy force. The second term is due to the pressure gradient in the fluid surrounding the particle. The third term is a drag force. The fourth term is a force to accelerate the virtual "added mass" corresponding to the surrounding fluid. The last term is the so-called "Basset" term, which is a memory effect term, which takes into account the deviation of the flow pattern from steady state. Equation 22, however, does not include the lift force, which is caused by the particle spin.

An analysis by Morrison and Stewart (1976) shows that the "Basset" term depends on the rate of change of the relative velocity. For flows in which the frequency of the oscillatory motion of the carrier fluid is small the Basset term can be neglected. Furthermore, Maxey and Riley (1983) have presented order of magnitude estimates for various forces acting in the bubble. They concluded that once the motion is established, the Basset history term is only of a secondary order when compared to other forces. Since in this study, we release the bubble with the same initial velocity as its surrounding liquid, we will neglect the "Basset" term.

Equation 22 describes the motion of a solid particle in a flow. For a gas bubble the mass of the gas inside the bubble can be neglected relative to the added mass of the fluid. To describe the motion of a gas bubble, however, one has to take into account the force due to the bubble volume variation. Johnson and Hsieh (1966) added the term necessary to consider the bubble volume variations as follows:

$$\frac{d\vec{U}_b}{dt} = -2\vec{g} + \frac{3}{\rho}\nabla p + \frac{3}{4}C_D\left(\vec{U} - \vec{U}_b\right) \mid \vec{U} - \vec{U}_b \mid + \frac{3}{R}\left(\vec{U} - \vec{U}_b\right)\dot{R}\,. \tag{25}$$

With a prescribed flow field, a Runge-Kutta fourth-order scheme can be applied to integrate Equations 22 and 20 or 21 through time to provide the bubble trajectory and its volume variation during bubble capture by the tip vortex.

The pressure in the liquid at a distance, l, from the bubble center is given by:

$$p = \frac{\rho}{l}\left[R^2\ddot{R} + 2R\dot{R}^2\right] - \rho\left[\frac{R^4\dot{R}^2}{2l^4}\right]. \tag{26}$$

Far away from the bubble the second bracketed term is negligible, and Equation 26 degenerates to the equation usually given to the acoustic pressure for instance by Fitzpatrick and Strasberg (1958):

$$p_a(t') = \frac{\rho\ddot{V}(t')}{4\pi l}, \qquad t' = t - \frac{l-R}{c}. \tag{27}$$

Since the bubble volume is $V = 4/3\pi R^3$ we have

$$p_a(t') = \frac{R\rho}{l}\left[R\ddot{R}(t') + 2\dot{R}^2(t')\right], \tag{28}$$

where p_a is the acoustic pressure and c is the sound speed.

10 Numerical Results

In the current study the computations are conducted by releasing bubbles at x=0 with zero velocity and an initial nucleus equilibrium condition, i.e. the initial gas pressure is determined by

$$p_{g0} = p_{\omega}(r) - p_v + \frac{2S}{R_0}. \tag{29}$$

Since the circulation at x=0 is assumed to be zero (see Figure 2), we have $p_{\omega}(r) = p_{\infty}$. By integrating Equations 21 and 22 the variation of bubble radius and acoustic pressure versus time can be obtained. Figure 3 shows an example of bubble radius history and acoustic pressure for a bubble of $R_0 = 10\mu m$ released at $D = 0.5a_c$ away from the vortex center in the model scale. To investigate the influence of the radial release location, *D*, on the solution, results are compared for different values of *D*. It is found that the acoustic pressure is insensitive to the initial bubble position when this position is close to the vortex axis, as shown in Figure 4. To be consistent, the results shown below are all obtained for the same release location, $D = 0.5a_c$.

While the solution is insensitive to the radial release location, the solution highly depends on the initial bubble size. Different R_0 led to different trajectories and thus cause the bubble to experience different pressure history. Figure 5 shows the trajectory and the encountered pressure for different initial bubble radius released from the same location. The maximum acoustic pressure measured at 30 cm from the vortex center versus the cavitation number for different initial bubble sizes is shown in Figure 6.

From an engineering viewpoint, cavitation inception is usually determined through visual or acoustical techniques. Inception is called when the measurement detects events above a pre-defined threshold. In the laboratory the most commonly used threshold is via visual observation when bubbles become visible. This visual technique can hardly be applied to full-scale tests where an acoustic technique is preferred. Therefore, to be consistent for both scales only the acoustic technique is used to determine the cavitation inception in the current study. The criterion used to define the cavitation inception is based on the acoustical signal. Using the curve of maximum acoustic pressure versus cavitation number, we can obtain the rate of pressure change with the cavitation number, $-dp/d\sigma$, as shown in Figure 7. The cavitation inception number can then defined as the largest cavitation number for which $-dp/d\sigma >> 1$; say $-dp/d\sigma > 100,$. By applying this criterion we can obtain the cavitation inception number σ_{im} and σ_{if} for the model scale and full scale respectively. The value of nuclei effect parameter, *G* is then determined by

$$G = \frac{\sigma_{if}}{\sigma_{im}} \left(\frac{\mathrm{Re}_m}{\mathrm{Re}_f} \right)^{0.4}. \tag{30}$$

To show the nuclei effect, the values of *G* are plotted versus the ratio of nuclei size between model and full scales in Figures 8a and 8b. It is found that the value of *G* could be greater, equal or less than 1. This nuclei effect leads to deviation from the traditional scaling law that increases as Rom differs from Rof.

Consider the case with the same nuclei distributions available in the model test facility and full-scale environment. As noted in Fig 8a for Rom/Rof =1, the values of *G* are found to be 1.061, 1.022, and 1.002 for Rom = 0.5 μm, 1.0 μm, and 10 μm, respectively. They are all greater than 1. This means that with the same nuclei distributions, water quality exhibits a stronger effect on the model than in the full-scale, especially with small nuclei sizes.

To have *G*=1, namely no nuclei effect between the model tests and the full-scale observations, the initial bubble size in the model test must be slightly greater than in the full-scale environment. Fig 8 gives Rom/Rof = 1.55, 1.6 and 1.85 for Rom = 0.5, 2.5, and 10 μm, respectively.

However, if the value of Rom/Rof is large and much greater than 1, the effect of the water tensile strength at cavitation inception will be relatively weaker in the model test than in full-scale observation and the values of *G* would be less than 1 as noted in Fig 8. On the other hand, if the values of Rom/Rof are much less than 1, the effect of the tensile strength at cavitation inception will be relatively strong at the model test than in full-scale observation and the values of *G* will be greater than 1 as noted in Fig 8b. This later case can occur if the model is tested in a lake or in a laboratory with low air contents.

11 Conclusion

Prediction of tip vortex cavitation inception on a hydrofoil or propeller still relies heavily on model tests and application of cavitation scaling. A simple method to scale the effects of model size and free stream nuclei on tip vortex cavitation inception has been developed and presented in this paper. Based on geometric, kinematics and dynamic similarity, circulation, core thickness, pressure distributions in a full-scale trailing vortex are obtained if the model data are given.

If boundary layers on model and full-scale are both turbulent, the effect of model size on tip vortex cavitation is shown to be related by $(Re_f / Re_m)^{0.4}$.

The effect of model size and nuclei on tip vortex cavitation is shown to be related by $\sigma_{if} / \sigma_{im} = G(Re_f / Re_m)^{0.4}$. It is found that the value of G could be greater, equal or less than 1. The nuclei effect, which leads to deviation from the traditional scaling law, is increased as as Rom differs from Rof .

Acknowledgements
The work was supported by NAVSEA 93R under the direction of Mr. Doug Dahmer. We appreciate very much of technical supports and discussions of Mr. Jude Brown and Dr. Han-Lieh Liu of NSWC Carderock Division.

References

Abbott, I. H. and Von Doenhoff A. E., Theory of Wing Sections, Dover Publications, Inc.
Arndt, R. E. A., 1981, Cavitation and fluid machinery and hydraulic structures, Ann. Rev. Fluid Mech. Pp273-328
Basset, A. B., 1888, A treatise on hydrodynamics, Vol 2, Ch5, Deighton, Bell and Co., Cambridge, England
Boussinesq,, J., 1903, Theorie analytique de la chaleur, Vol 2, P224, Gautheir-Villars, Paris
Brennen C. E., 1995, Cavitation and Bubble Dynamics, Oxford University Press
Fitzpatrick, N. and Strasberg, M., 1958, Hydrodynamic sources of sound, 2nd Symp. of Naval Hydrodynamics, pp 201-205
Fruman D. H., Dugue C., and P. Cerruti, 1991, Tip vortex roll-up and cavitation, ASME Cavitation and multiphase flow forum, pp 43-48
Fruman D. H., Castro F., Pauchet A. and Pichon T. 1994, On tip vortex turbulence, wandering and cavitation occurrence, The 2nd International Symp. On Cavitation, Tokyo, Japan
Gilmore, F. R., 1952, Calif. Inst. Technol. Eng. Div. Rep 26-4, Pasadena, Ca.
Green S. L. and A. J. Acosta, 1991, Unsteady flow in trailing vortices, J. Fluid Mech. Vol 227, pp 107-134
Hsiao, C-T, Chahine, G.L., and Liu, H.L., 2000, "Scaling effects on bubble dynamics in a tip vortex flow: Prediction of cavitation inception and noise", DYNAFLOW, INC. Technical Report 98007-1nswc.
Hsiao, C-T, Chahine, G.L., and Liu, H.L., 2001, "Scaling effect on prediction of cavitation inception in a line vortex flow", submitted to Journal of Fluid Engineering.
International Towing Tank conference, 1990, 19th ITTC Cavitation Committee Report, Madrid, Spain
Liang, X. and B. R. Ramaprian, 1991, Visualization of the wing-tip vortex in temporal and spatial pressure gradients, JFE Vol 113 pp 513-515
Maxey, M. R., and Riley, J. J., 1983, Equation of motion for a small rigid sphere in a nonuniform flow, Phys. Fluids, Vol 26, pp 883-889
McCormick, B. W.,1954, "A study of the minimum pressure in a trailing vortex system," Ph.d dissertation, Penn State University
McCormick, B. W., 1962, On cavitation produced by a vortex trailing from a lifting surface, J. Basic Eng. Pp 369-370
Oseen, C. W., 1927, Hydrodynamik, p132, Leipzig
Plesset, M. S.,1948, Dynamics of cavitation bubbles, J. of Applied Mechanics, Vol 16, pp 228-231
Schlichting, H., 1979, Boundary Layer Theory, McGraw-Hill Book Co.

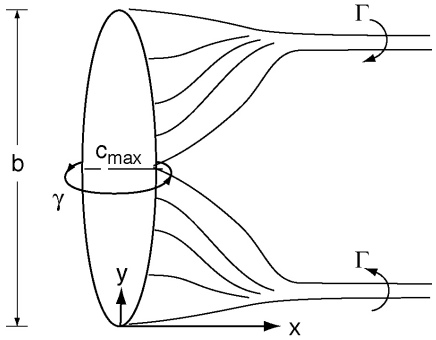

Figure 1. Sketch of a Hydrofoil.

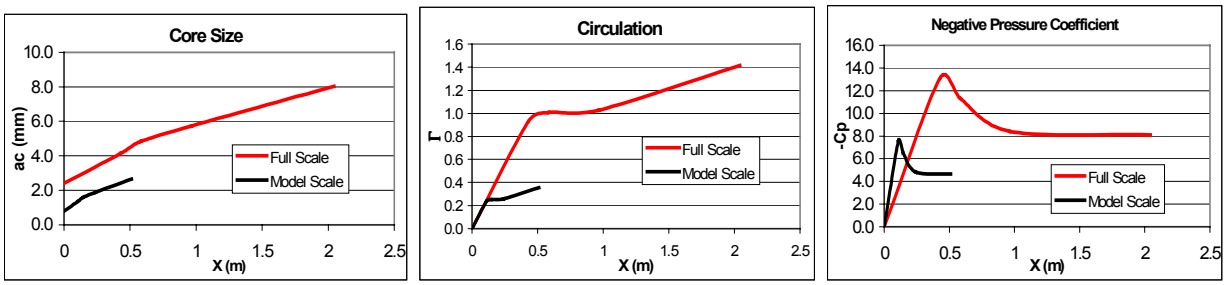

Figure 2. Vortex core size and circulation distribution in the selected trailing vortex as a function of x.

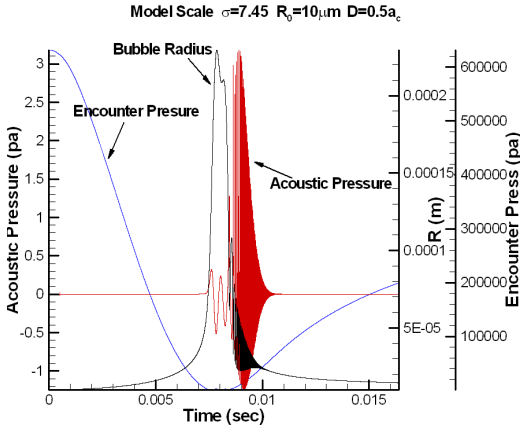

Figure 3. An example of the encountered pressure, bubble radius history and acoustic pressure.

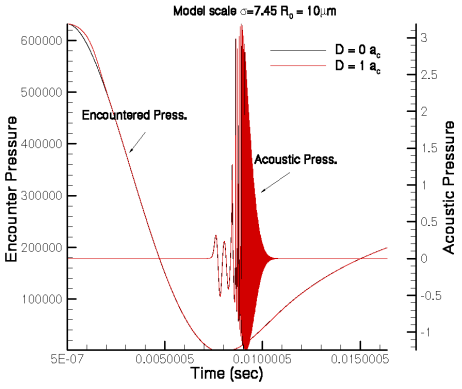

Figure 4. Different release locations only slightly change the encountered pressure at the beginning. The acoustical pressure curves are almost identical.

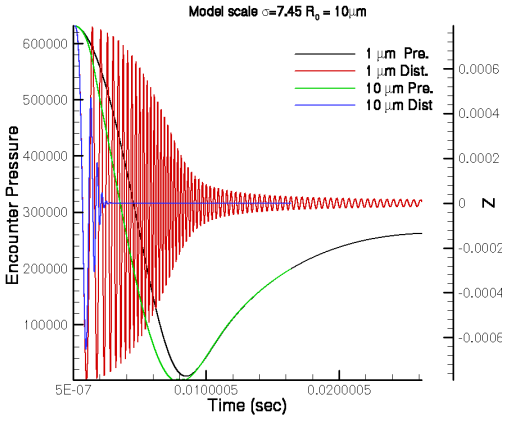

Figure 5. Different trajectories and encountered pressures for different initial bubble radii released from the same location.

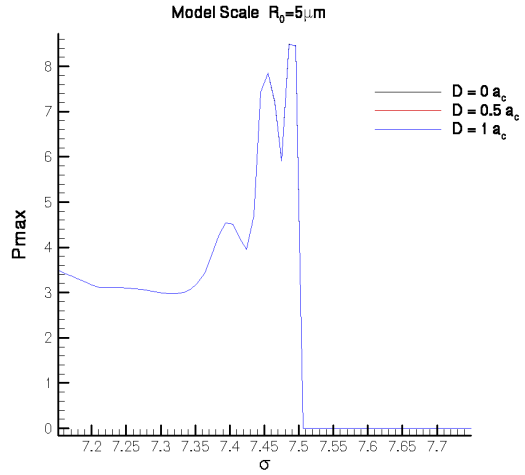

Figure 6. The curves of maximum acoustical pressure versus cavitation number for different release locations are identical

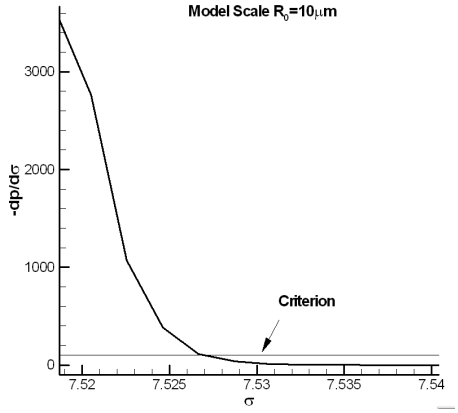

Figure 7. Based on the acoustical signal the cavitation inception number is defined when $-dp/d\sigma$ becomes larger than a certain value, here >100.

(a) (b)

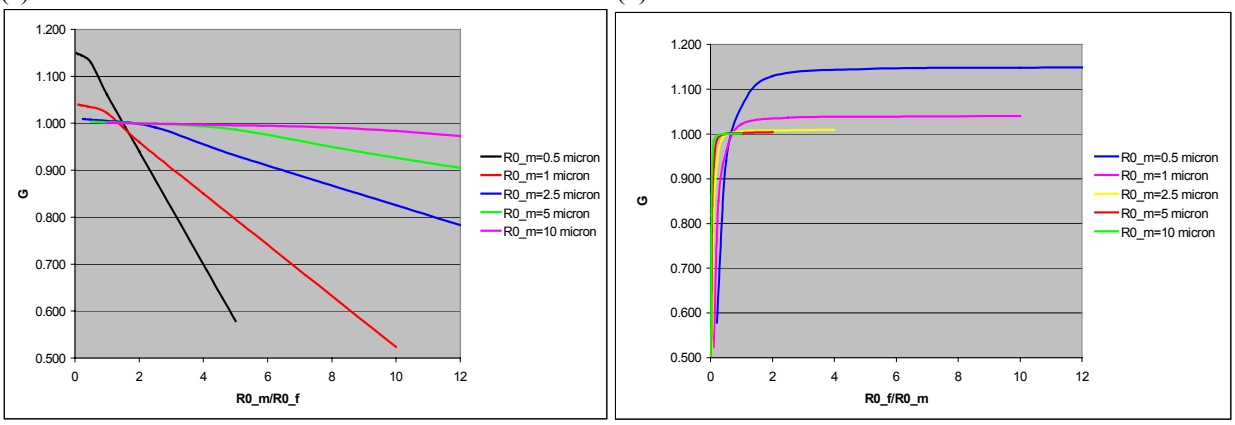

Figure 8. Curves of the nuclei parameter G versus R0_m/R0_f and R0_f /R0_m for different initial bubble radii. Indices m and f are for model and full scale